THE JOURNAL OF PHYSICAL CHEMISTRY C

Article

Cite This: J. Phys. Chem. C 2018, 122, 15118−15124

pubs.acs.org/JPCC

Two-Dimensional Tetragonal Titanium Carbide: a High-Capacity and High-Rate Battery Material

Dong Fan,[†,§] Shaohua Lu,*[,†,§] Yundong Guo,[‡] and Xiaojun Hu*[,†]

[†]College of Materials Science and Engineering, Zhejiang University of Technology, Hangzhou 310014, China

[‡]School of Engineering and Technology, Neijiang Normal University, Neijiang 641000, China

Supporting Information

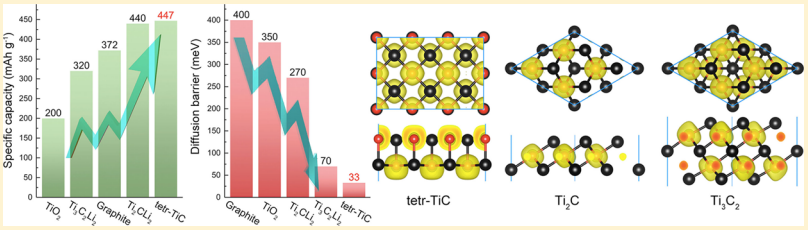

ABSTRACT: High-performance electrode materials are critical for the development of next-generation energy conversion and storage systems. Herein, we report a theoretical design of novel two-dimensional materials, namely, tetragonal titanium carbide and nitride (tetr-TiC and tetr-TiN) based on ab initio calculations. State-of-the-art calculations show that tetr-TiC and tetr-TiN deliver the intrinsic metallic nature, high thermal stability, and satisfactory lithium-ion storage and rate capability. More importantly, compared with previously known Ti_3C_2 and Ti_2C sheets, the proposed new material has lower Li diffusion barrier, higher theoretical capacity, and lower average open circuit. Combining such advanced features, the proposed tetragonal TiC is a promising candidate for future lithium-ion batteries, supercapacitors, and fuel cells.

INTRODUCTION

The design and development of new electrochemical energy storage (EES) systems are crucial for future clean energy economy. It has been well accepted that breakthroughs in EES devices require innovative electrode materials because of conventional lithium ion batteries (LIBs) based on graphite anodes no longer provide satisfactory storage capacity and performance.[1,2] Among all possible candidates for high-performance and ultrastable anode materials, transition-metal carbides (TMCs) and nitrides (TMNs) are promising candidates for applications in energy conversion and storage devices such as photovoltaic cells, LIBs, and supercapacitors.[3−5] However, in the light of high ion conductivity and fast chemical reactivity, bulk TMCs and TMNs are suggested with low performances than its nanostructured counterparts.[6]

Meanwhile, following the successful exfoliation of graphene, the two-dimensional (2D) concept also has extended to TMC and TMN families. A new group of 2D early TMCs was proposed by Naguib et al., MXenes, namely.[7] Since then, many reports were focused on their potential applications as promising candidates for LIBs and electrochemical capacitors, in view of their rich chemistries and morphologies.[7,8] Experimentally, the usual strategy to synthesize MXenes is selective etching of the A element from the $M_{n+1}AX_n$ phase, where M is an early transition metal, A is mainly a group iiiA or ivA metal, X is C and/or N, and n = 1, 2, or 3.[9] Till now, more than 44 MXenes variants have been theoretically proposed. Among them 19 has been successfully synthesized, including Ti_3C_2, Ti_2C, Nb_2C, V_2C, $(Ti_{0.5}Nb_{0.5})_2C$, $(V_{0.5}Cr_{0.5})_3C_2$, Ti_3CN, and Ta_4C_3.[7−10] The wide chemical and structural diversity of MXenes facilitates the property tuning for applications in many fields such as photovoltaic cells, LIBs, supercapacitors, and chemical catalysis.[7−10] Previous theoretical and experimental studies have identified that MXenes are superior LIB anodes with low diffusion barriers and relatively high storage capacity.[3,7−9] However, the MXene monolayer structure is not indefinitely stable, especially operated in oxygen and water environments, under which leads to the formation of metal oxide nanocrystals (i.e., TiO_2), decorating the sheet edges.[11−13] For this reason, our research objective is identifying alternative stable 2D TiC with both high capacity and rate capability.

In this work, by means of density functional theory (DFT) computations, we report a theoretical design of hitherto unknown, yet simple 2D materials, tetr-TiC and tetr-TiN sheets, namely. We show that tetr-TiC is a global minimum structure in 2D space by performing particle swarm optimization structure search. Moreover, this energetic favorable behavior holds a promise to realize experimentally. Finally, we investigated the Li storage capability in tetr-TiC and tetr-TiN sheets to explore their potential applications as anode materials for LIBs.

Received: April 11, 2018
Revised: June 20, 2018
Published: June 20, 2018

DOI: 10.1021/acs.jpcc.8b03425
J. Phys. Chem. C 2018, 122, 15118−15124

METHODS

All structural relaxations were carried out with the projector-augmented wave potentials and Perdew–Burke–Ernzerhof (PBE) generalized gradient approximation[14] as implemented in the Vienna ab initio simulation package (VASP).[15] The $2s^2 2p^2$, $3d^3 4s^1$, and $2s^1$ atomic orbitals were treated as valence states for C, Ti, and Li, respectively. A 650 eV cutoff energy was used for the plane-wave basis set. Especially, the DFT-D2 method of the Grimme van der Waals (vdW) correction[16] was used to accurately account for the long-range interactions between Li atom on structures. We ensured at least 15 Å vacuum regions between two adjacent sheets and considered vdW interactions to investigate the Li adsorption and diffusion on tetr-TiC (tetr-TiN) sheet using a 3 × 3 supercell with one adsorbed Li atom. After full structural optimization, a denser k grid of 24 × 24 and 14 × 14 was employed in the calculation of density of states (DOS) by using PBE and Heyd–Scuseria–Ernzerhof (HSE06)[17] functionals, respectively. Note that standard DFT calculations at PBE level are well-known to underestimate the band gaps; we utilize HSE06 functional to calculate the corrected band structure. The search for the ground-state structure of ultrathin TiC films was performed in the CALYPSO package,[18,19] which has been successfully applied to various crystal surfaces and low-dimensional materials,[20−22] and is a leading structure prediction method in the field. The number of structures in each generation was maintained at 40. Total atoms of 4, 6, 8, and 10 per unit cells were considered in structure search.

The cohesive energy (E_{coh}) and molar formation energy (δF) for proposed structures was evaluated by[22]

$$E_{coh} = \frac{E_{total}}{n} - x(E_{Ti}) - (1-x)E_C$$

$$\delta F = \frac{E_{total}}{n} - x(\mu_{Ti}) - (1-x)\mu_C$$

where E_{coh} denotes the cohesive energy of corresponding 2D structures and δF is the molar formation energy of 2D TiC systems, respectively; E_{Ti}, E_C, and E_{total} are the total energies of a single Ti atom, a single C atom, and 2D TiC compounds, respectively; n is the total number of atoms in supercell; μ_{Ti} and μ_C represent chemical potentials of titanium and carbon in bulk counterparts, respectively.

Phonon dispersions were calculated on the basis of density functional perturbation theory as implemented in the phonopy code.[23] Ab initio molecular dynamics (AIMD) simulations were performed in an *NVT* ensemble.[24] The climbing-image nudged elastic band method[25] was employed to locate the minimum-energy path and diffusion energy barrier of Li atom diffusion on tetr-TiC and tetr-TiN sheets. To quantify the stability of the isolated Li atom adsorption on the surface of 3 × 3 supercell, the adsorption energy was calculated by using the following equation

$$E_{ad} = E_{total} - E_{Li} - E_{(tetr\text{-}TiC(N))}$$

where E_{ad}, E_{Li}, and $E_{(tetr\text{-}TiC(N))}$ are total energies of Li-adsorbed tetr-TiC (tetr-TiN), a Li atom (in bulk phase), and tetr-TiC (tetr-TiN), respectively.

Considering that the charging/discharging processes of TiC sheet anode can be assumed as:

$$TiCLi + xLi^+ + xe^- \leftrightarrow TiCLi_x$$

thus, the average open circuit voltage (OCV) was estimated by (volume and entropy effects are neglected)

$$OCV \approx \frac{E_{tetr\text{-}TiC(N)} + xE_{Li} - E_{tetr\text{-}TiC(N)Li_x}}{x}$$

where $E_{tetr\text{-}TiC(N)}$, $E_{tetr\text{-}TiC(N)Li_x}$, and E_{Li} are the potential energies of tetr-TiC (tetr-TiN), tetr-$TiCLi_x$ (tetr-$TiNLi_x$), and metallic Li bulk, respectively.

RESULTS AND DISCUSSION

Atomic Configurations and Stabilities. The global structure search with both variable layer-thickness and cell-sizes is performed to screen low-energy 2D TiC structures, as implemented in the CALYPSO package. After large-scale global structure search, we successfully obtained the lowest energy geometries of tetr-TiC and multilayer tetr-TiC sheets. Figure 1a presents the structure pattern of the newly proposed

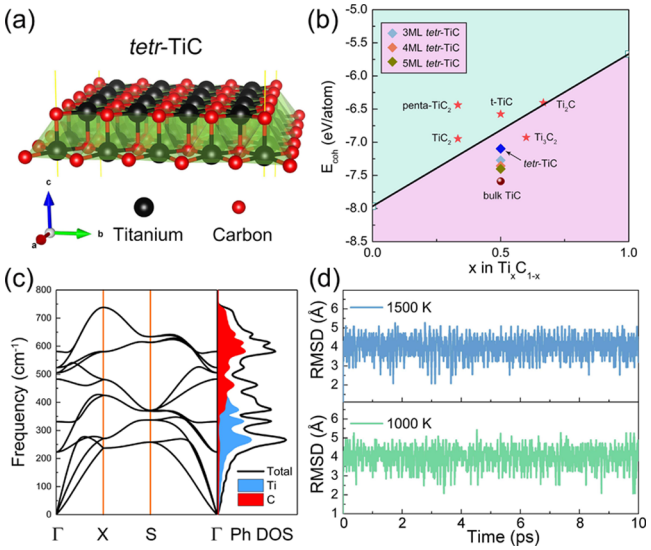

Figure 1. (a) Optimized geometries of the free-standing tetr-TiC sheet. (b) Calculated cohesive energy (E_{coh}) for the ground state Ti_xC_{1-x} sheet as the function of x. A straight line connects E_{coh} of graphene and bulk Ti at x = 0 and 1. (c) Phonon dispersion curves of tetr-TiC along the q-path of Γ–X–S–Γ (left) and the corresponding partial phonon DOS (right). (d) Fluctuations of rmsd of tetr-TiC 4 × 4 supercell as a function of the AIMD step at 1000 and 1500 K. The trajectories of the structures are stable over the entire simulation time at different temperatures.

2D TiC sheet (labeled as tetr-TiC). Different from multilayer hexagonal MXenes,[7] Ti and C atoms in this sheet are arranged in a tetragonal lattice, and the optimized lattice parameters are $a = b$ = 2.99 Å. The calculated length of Ti–C bond of tetr-TiC is 2.12 (2.16) Å along the horizontal (vertical) direction, close to the corresponding bond length in bulk phase TiC (2.16 Å) and significantly larger than the previously proposed metastable t-TiC (2.02 Å).[26] In view of structural similarity, we also design the tetragonal titanium nitride, labeled as tetr-TiN, as show in Figure S1. In the following section, we will systematically investigate the stabilities, electronic properties, and the performance of LIBs of tetr-TiC and tetr-TiN sheets.

From energy point of view, we first calculate the cohesive energy of tetr-TiC and compare it with other previously proposed Ti_xC_{1-x} compounds, that is, Ti_3C_2, Ti_2C, TiC_2, and TiC bulk, as illustrated in Figure 1b. We find that tetr-TiC

DOI: 10.1021/acs.jpcc.8b03425
J. Phys. Chem. C 2018, 122, 15118−15124

(−6.98 eV/atom) is energetically more favorable than the previously proposed TiC monolayer (−6.45 eV/atom).[26] This indicates that the 2D Ti−C system (with 1:1 stoichiometry) prefers to be this tetragonal bilayer group. We also calculate the molar (per atom) formation energy (δF) to further assess the relative stability of the proposed new structures. Figure S2 plots the δF for Ti_xC_{1-x} as the function of x. The tetr-TiC and multilayer tetr-TiC (see the structure pattern in Figure S3) show stable phases as the δF are well below the straight line with negative values of −0.27 and −0.44 to −0.58 eV, respectively. In contrast, the additional calculated δF for the penta-TiC_2, TiC_2,[27] and t-TiC are 0.77, 0.26, and 0.25 eV (0.24 in ref 26), respectively. Therefore, the relatively lower cohesive energy and δF ensure that tetr-TiC is a strongly bonded sheet.

We then calculate the phonon dispersion spectra and DOS to check the dynamical stability of tetr-TiC (tetr-TiN) sheet. Evident from Figures 1c and S4, the absence of imaginary vibrational frequencies within the entire Brillouin zone demonstrates that tetr-TiC and tetr-TiN are also dynamically stable. Importantly, the highest frequency of tetr-TiC and tetr-TiN reach up to 737 and 668 cm^{-1}, which are higher than those of MoS_2 (473 cm^{-1}),[28] silicene (580 cm^{-1}),[29] arsenene (≈225 cm^{-1}), and antimonene (≈325 cm^{-1}),[30] indicating robust Ti−C and Ti−N bonds in their structures. For tetr-TiN, two significant phonon gaps are clearly observed, splitting the vibrational modes into the low-frequency (0−331 cm^{-1}) and the high-frequency (375−509 and 547−667 cm^{-1}) ranges. The detailed analysis of partial phonon DOS indicates that the high-frequency modes of tetr-TiC and tetr-TiN sheets are entirely contributed by the C and N atoms, respectively. Furthermore, we performed AIMD simulations using a canonical (NVT) ensemble to check the thermal stability of the proposed structures. A relatively large 4 × 4 supercell is used in all simulations at 1000 and 1500 K, respectively. Figure S5 summarizes the evolution of total energy of tetr-TiC and tetr-TiN at 1500 K, respectively. After heating at 1500 K for 10 ps with a time step of 1 fs, no structure reconstruction is found in all of the simulation processes. The thermal stability of structures is also identified by analyzing the backbone root-mean-square deviation (rmsd) from the starting crystal configuration over the process of the trajectory. As seen in Figure 1d, it is evident that the rmsd levels off to ∼4.0 Å for tetr-TiC sheet at 1000 and 1500 K, indicating that the geometric configuration is expected to be highly stable.

The capability of forming a freestanding membrane is another important parameter to evaluate the stability of 2D materials. To explore if it is strong enough to resist mechanical deformations, we calculate the in-plane stiffness of tetr-TiC and tetr-TiN. As a validation of the calculation method, the repeated calculations of elastic constants for Ti_2C are $C_{11} = C_{22}$ = 130 GPa and $C_{12} = C_{21}$ = 34 GPa, which are in agreement with previous results.[31] Generally, for a mechanically stable 2D structure, the elastic constants need to satisfy $C_{11}C_{22} - C_{12}C_{21} > 0$ and $C_{66} > 0$ 0.[22,32] Considering the tetragonal symmetry of tetr-TiC(N), the elastic constants values only need to be satisfied with $C_{11} > |C_{12}|$ and $C_{66} > 0$. As shown in Table S1, the calculated elastic constants of tetr-TiC and tetr-TiN are in agreement with the mechanical stability criterion for 2D sheets, demonstrating that the strictures are strong enough to keep a stable freestanding configuration without the support of a specific substrate.

Electronic Property. As shown in Figures 2 and S1, the nonzero DOS at the Fermi energy demonstrate the metallic

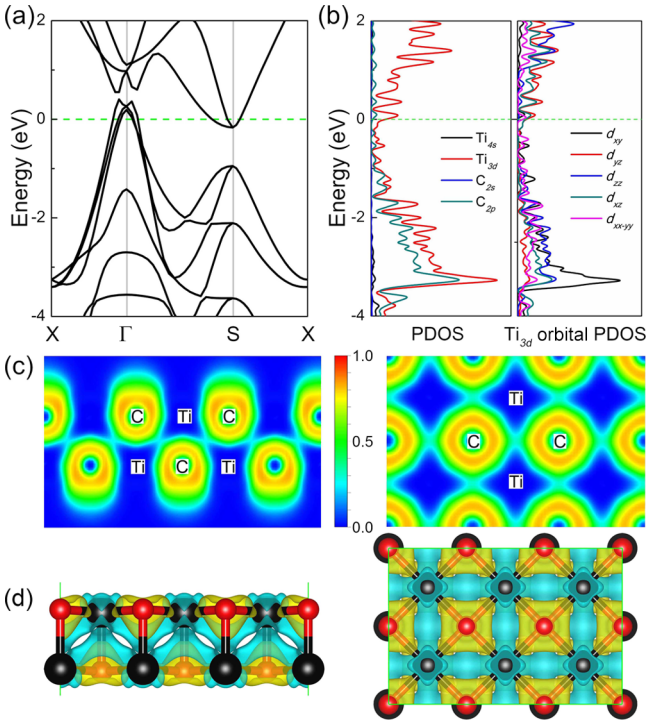

Figure 2. (a) Electronic band structure and (b) partial DOS of tetr-TiC at equilibrium state. Dashed lines denote the Fermi level. (c) Plot of the corresponding ELF maps viewed from the horizontal and vertical directions. ELF ranges from 0.0 (blue) to 1.0 (red). (d) Side and top views of deformation charge density for tetr-TiC. The isosurfaces value is 0.01 a.u. Yellow and blue clouds represent electron increasing and reducing zones, respectively.

properties of tetr-TiC and tetr-TiN. Generally, the interlayer interaction will also affect the band structures of 2D materials. To interpret the origin of the metallicity of tetr-TiC, we also plotted the projected DOS onto the atomic orbitals of the Ti and C atoms in the unit cell, as illustrated in Figure 2b. The energy bands near the Fermi level are mainly contributed by Ti_{3d} stats, whereas the Ti_{4s}, C_{2s}, and C_{2p} give only a small contribution to the metallic behavior. Detailed projected DOS analysis also reveals that the hybridized Ti_{3d} and C_{2p} states are mainly distributed in the energy region below the Fermi level (from −1.5 to −3.5 eV). The concomitant electric conductivity is in line with good electron delocalization as revealed by electron localization function (ELF) and deformation electron density (DED) analyses (see Figures 2 and S6). The DED result reveals clearly electron transformation from Ti to C(N) atom. For tetr-TiC and tetr-TiN, Bader charge analysis[33] suggests a charge transfer of 1.49 and 1.50e from each Ti atom to C and N atoms, respectively.

Li Adsorption and Diffusion. It is well accepted that the performance of charging/discharging process and circulation efficiency in LIBs is strongly dependent on the diffusion rate of Li atom on the anode surface. Therefore, we inspect the isolated Li adsorption and diffusion behaviors on the corresponding surface using a 3 × 3 supercell. To examine the most favorable adsorption configuration of Li atom on the surfaces, we consider two possible adsorption sites of a single Li atom on supercell and calculated the corresponding

DOI: 10.1021/acs.jpcc.8b03425
J. Phys. Chem. C 2018, 122, 15118−15124

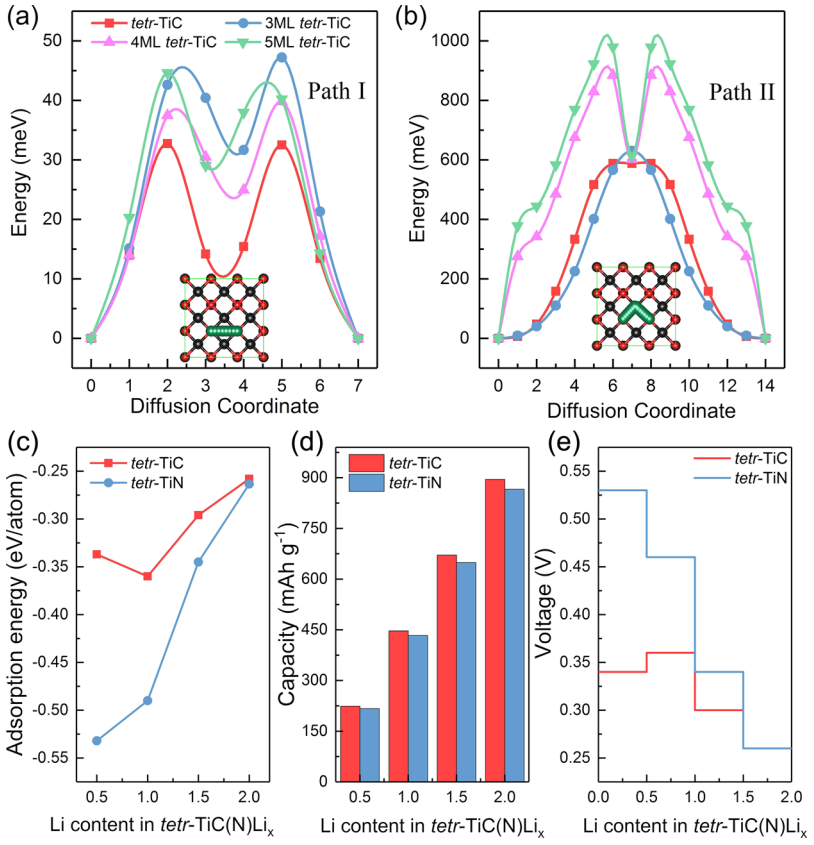

Figure 3. Energy profile of lithium diffusion along path I (a) and path II (b) for tetr-TiC and multilayer tetr-TiC in 3 × 3 supercell. The inserted schematic illustrates the top view of the considered migration paths for Li diffusion. (c) Variation of adsorption energy with increasing Li content in tetr-TiC(N). (d) Li theoretical capacities as a function of the adsorbed Li content in tetr-TiC(N). (e) Calculated voltage profile as a function of Li concentration in tetr-TiC(N) sheet for double-side adsorption.

adsorption energy for the most stable adsorption site (on top of C atom). The charge difference maps of two high-symmetry sites for tetr-TiC and tetr-TiN are presented in Figure S7. The calculated distance between Li and C atoms and the adsorption energy on tetr-TiC and tetr-TiN sheets are 2.00, 1.92 Å and −0.16, +0.31 eV/atom, respectively.

We find that the calculated absorption energy of tetr-TiN is positive (Li bulk phase is used as a reference state) using DFT-D2 corrected functional, which means that a single Li ion does not prefer to absorb on its surface. However, when the Li concentration increases, the adsorption of Li atoms strengthens and becomes negative with adsorption of four Li atoms (see Figure S8, also observed the same trend by DFT-D3 method[34]). To further investigate the origin of this transformation, we performed DED analysis with multi-Li adsorbed conditions compared with a single Li atom adsorbed system. As shown in Figure S9, when four Li atoms are adsorbed on 3 × 3 supercell of tetr-TiN, the adsorption energy decreases from +0.31 (a single Li atom adsorbed on a 3 × 3 system) to −0.05 eV/atom; DED analysis reveals that more electrons transfer from the adsorbed Li to the substrate, resulting in the decreasing of Li absorption energy. This observed electron transfer agrees with the larger electronegativity of nitrogen (3.04) than lithium (0.98). Simultaneously, when two adsorbed Li atoms are closer to each other, the system shows more energetically favorable and charge transfer (see Figures S9 and S10), which also demonstrates that tetr-TiN prefers to absorb multi-Li atoms. For this reason, we also evaluate the diffusion barrier of tetr-TiN with 4-Li adsorbed, as shown in Figure S11. Clearly, the calculated diffusion barrier is much higher than that of tetr-TiC sheet. Therefore, the tetr-TiC provides better performance than tetr-TiN, and we mainly discuss the advantages of tetr-TiC sheet in this work.

When the Li atom concentration further increases, the adsorption of Li atoms continuously weakens due to the enhanced Li−Li repulsion (see Figure 3c). The diffusion path and barrier of Li on the electrode material is indispensable to evaluate their potentials in LIBs. As illustrated in Figures 3 and S12, two diffusion pathways (path I, and path II) are considered. Obviously, a potential diffusion barrier (33 meV) for one Li atom on tetr-TiC surface (path I) was much lower than that in all previously proposed Ti_xC_{1-x} (70−270 meV), TiO_2 (350−650 meV), commercialized graphite anode materials (≈400 meV), or 3ML tetr-TiC (47.21 meV, see Figure S13). Thus, tetr-TiC could provide higher charge/discharge rates than these 2D materials.

Average OCV and Li Storage Capacity. As shown in Figure 3c, tetr-TiC possesses an adsorption energy of −0.258 eV/atom even at $x = 2$, suggesting the high stability of this adsorption state under high Li-concentration conditions. In comparison, tetr-TiN also can hold Li atoms in $TiNLi_2$ with an adsorption energy of −0.263 eV. As Li-adsorbed tetr-TiC(N)Li_x represents the high stability, we then evaluate the theoretical Li storage capacity and the average OCV of the free-standing tetr-TiC and tetr-TiN, as illustrated in Figure 3d,e, respectively.

Table 1 summarizes a comparison of the calculated specific capacity, diffusion barrier, and OCV with several potential

DOI: 10.1021/acs.jpcc.8b03425
J. Phys. Chem. C 2018, 122, 15118−15124

Table 1. Comparison of the Theoretical Specific Capacity (mA h g^{-1}), Diffusion Barrier (meV), and the Average OCV (V) of Candidate Anode Materials for the Li Ion Battery[a]

	theoretical specific capacity		diffusion barrier		OCV	
materials	Theor.	Expt.	Theor.	Expt.	Theor.	references
tetr-TiCLi	447	–	33	–	0.36	this work
tetr-TiNLi	433	–	266	–	0.46	this work
Ti_2CLi_2	440	–	270	–	0.44	35
$Ti_3C_2Li_2$	320	–	70	–	0.62	3
TiO_2	<200	200	350–650	350	1.5–1.8	36,38
graphite	372	372	400	–	0.23	39

[a]"–" means data unavailable.

anode materials in LIBs. For the one-layer adsorption of Li atoms, the theoretical specific capacities are found to be 447 and 433 mA h g^{-1} for tetr-TiCLi and tetr-TiNLi, respectively, which is comparable to the proposed Ti_2C and V_2C (440 and 419 mA h g^{-1}).[35] On the other hand, the estimated OCV and theoretical capacity of tetr-TiCLi_2 reach 0.26 V and 895 mA h g^{-1} in two-layer absorption, respectively. It should be noted that the capacity of tetr-TiC(N)Li_x at high concentration (x = 2) is almost two times larger than that of the commercialized graphite anode material. It is well accepted that the OCV should be located in the range of 0.1–1.0 V for an anode material.[40] In our study, as we increase the Li concentration from x = 0.5 to x = 2, the OCV decreases from 0.34 (0.53) to 0.26 (0.26) V for tetr-TiC(N), which is between those of the commercial anode materials, such as 0.23 V for graphite and 1.5–1.8 V for TiO_2.[37,39,41] Therefore, we demonstrate that tetr-TiC and tetr-TiN are promising next-generation high-performance anode candidates for LIBs because of their advanced electronic conductivity, smaller OCV, and improved Li-ion specific capacity.

Desirable Growth Substrate. Advanced growth techniques, such as molecular-beam epitaxy and migration-enhanced encapsulated growth methods should be possible for tetr-TiC(N) synthesis.[44] As an example, we theoretically explore possible substrates that facilitate epitaxial growth of tetr-TiC. We perform an extensive search on various materials, including both metal and semiconductor. The detailed structures of the tetr-TiC and substrate systems are illustrated in Figure 4. The lattice mismatch (δ) is defined as $\delta = [(L_{\text{tetr-TiC}} - L_{\text{sub}})/L_{\text{tetr-TiC}}] \times 100\%$, where $L_{\text{tetr-TiC}}$ and L_{sub} are the corresponding lattice parameters of the tetr-TiC and substrate, respectively. The corresponding lattice mismatches along the lattices of substrates and adsorption energies are also present. The adsorption energies of tetr-TiC on four considered substrates are negative, indicating that such structures once formed are preferably to be the most stable configuration. Considering the lattice mismatches and adsorption energies of the four promising substrates, the growth of tetr-TiC on the Au(100) and Sn(100) should be the most desirable.

CONCLUSIONS

To summarize, we have designed previously unrecognized class of new 2D material with intrinsic metal properties, namely, the tetragonal TiC and TiN sheets. Further first-principle calculations showed that these two structures are mechanically and dynamically stable. Especially, a global minimum search for 2D TiC with 1:1 stoichiometry revealed that tetr-TiC is the global lowest-energy structure on the potential energy surface, which endows tetr-TiC great possibility to be synthesized in the laboratory. Using a series of theoretical methods, we demonstrate that tetr-TiC and tetr-TiN exhibit exceptional properties including high stabilities, metallic properties, fast Li-ion diffusion rate and shorter diffusion length, high theoretical capacity, and small average open voltage. Our study not only highlights the advantages of tetr-TiC as the next generation of EES devices beyond the commercially used graphite electrode but also encourages further experimental investigations on the tetragonal phases of 2D TMC and TMN materials.

Note that we have further identified the dynamic stability of several typical 2D early TMCs and TMNs, labeled as tetr-TMXs (where "M" is an early transition metal, that is, Sc, Ti, V, Sr, Zr, Nb, Ta, Hf, and "X" is C or N), by calculating phonon dispersion curves (see Figures S14–S16). Further studies can be done to explore the electronic properties and Li

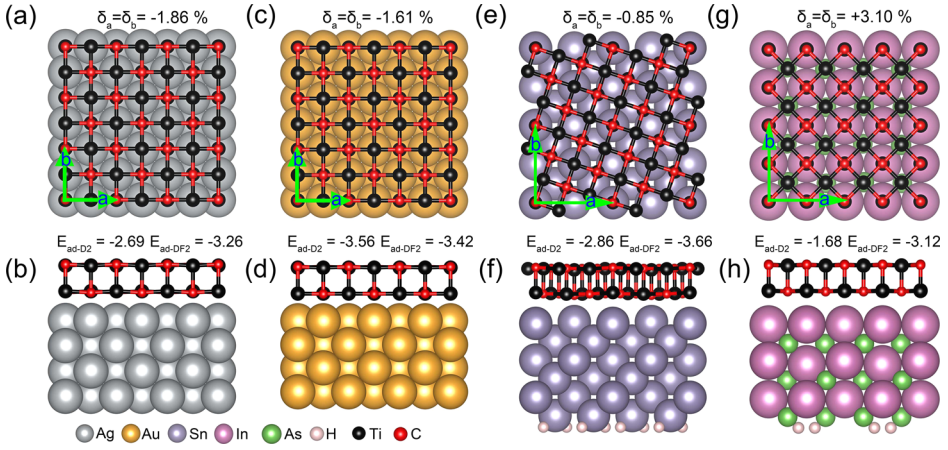

Figure 4. Top views of the respective tetr-TiC on (a) Ag(100), (c) Au(100), (e) Sn(100), and (g) InAs(100). The corresponding side views are given in the lower panels. Comparisons of the lattice mismatches and adsorption energies of tetr-TiC on the corresponding substrates. Here, a (b) is the lattice constant of the corresponding substrate, the different δ (%) values measure the different lattice mismatches for the systems, and E_{ad} measures the corresponding adsorption energies (per unit cell). The sub-script of the adsorption energy indicates the vdW correction scheme (by using DFT-D2 and vdW-DF2[42,43] methods).

DOI: 10.1021/acs.jpcc.8b03425
J. Phys. Chem. C 2018, 122, 15118–15124

storage capability of other tetr-TMXs based on the structures reported in this work.

■ ASSOCIATED CONTENT

Supporting Information

The Supporting Information is available free of charge on the ACS Publications website at DOI: 10.1021/acs.jpcc.8b03425.

Elastic constants, in-plane stiffness and Poisson's ratios of the proposed tetr-TiC and tetr-TiN; band structure of tetr-TiN; calculated molar formation energy for the ground state Ti_xC_{1-x} sheet as the function of x; phonon dispersion curves of tetr-TiN; fluctuations of total energy of tetr-TiC (tetr-TiN) supercell as a function of the AIMD step at 1500 K; charge density difference plots of the single and four Li adsorbed tert-TiN; and phonon band structures of other tetr-TMXs (PDF)

■ AUTHOR INFORMATION

Corresponding Authors

*E-mail: lsh@zjut.edu.cn. Phone: +86-571-88871522. Fax: +86-571-88871522 (S.L.).

*E-mail: huxj@zjut.edu.cn (X.H.).

ORCID

Dong Fan: 0000-0003-1873-3416

Xiaojun Hu: 0000-0001-7851-9900

Author Contributions

§D.F. and S.L. contributed equally.

Notes

The authors declare no competing financial interest.

■ ACKNOWLEDGMENTS

This work was supported by the National Natural Science Foundation of China (grant nos. 11504325, 50972129, and 50602039) and Natural Science Foundation of Zhejiang Province (LQ15A040004). This work was also supported by the international science technology cooperation program of China (2014DFR51160), the National Key Research and Development Program of China (no. 2016YFE0133200), the European Union's Horizon 2020 Research and Innovation Staff Exchange (RISE) Scheme (no. 734578), and the One Belt and One Road International Cooperation Project from Key Research and Development Program of Zhejiang Province (2018C04021).

■ REFERENCES

(1) Ji, L.; Lin, Z.; Alcoutlabi, M.; Zhang, X. Recent developments in nanostructured anode materials for rechargeable lithium-ion batteries. *Energy Environ. Sci.* **2011**, *4*, 2682−2699.

(2) Zhao, Z.; Liu, L.; Yu, T.; Yang, G.; Bergara, A. Pressure-Induced Stable Li5P for High-Performance Lithium-Ion Batteries. *J. Phys. Chem. C* **2017**, *121*, 21199−21205.

(3) Tang, Q.; Zhou, Z.; Shen, P. Are MXenes Promising Anode Materials for Li Ion Batteries? Computational Studies on Electronic Properties and Li Storage Capability of Ti3C2 and Ti3C2X2 (X = F, OH) Monolayer. *J. Am. Chem. Soc.* **2012**, *134*, 16909−16916.

(4) Zhao, S.; Kang, W.; Xue, J. Role of strain and concentration on the li adsorption and diffusion properties on Ti2C layer. *J. Phys. Chem. C* **2014**, *118*, 14983−14990.

(5) Wang, D.; Gao, Y.; Liu, Y.; Jin, D.; Gogotsi, Y.; Meng, X.; Du, F.; Chen, G.; Wei, Y. First-Principles Calculations of Ti2N and Ti2NT2 (T = O, F, OH) Monolayers as Potential Anode Materials for Lithium-Ion Batteries and Beyond. *J. Phys. Chem. C* **2017**, *121*, 13025−13034.

(6) Zhong, Y.; Xia, X.; Shi, F.; Zhan, J.; Tu, J.; Fan, H. J. Transition metal carbides and nitrides in energy storage and conversion. *Adv. Sci.* **2016**, *3*, 1500286.

(7) Naguib, M.; Kurtoglu, M.; Presser, V.; Lu, J.; Niu, J.; Heon, M.; Hultman, L.; Gogotsi, Y.; Barsoum, M. W. Two-dimensional nanocrystals produced by exfoliation of Ti3AlC2. *Adv. Mater.* **2011**, *23*, 4248−4253.

(8) Naguib, M.; Mashtalir, O.; Carle, J.; Presser, V.; Lu, J.; Hultman, L.; Gogotsi, Y.; Barsoum, M. W. Two-dimensional transition metal carbides. *ACS Nano* **2012**, *6*, 1322−1331.

(9) Naguib, M.; Mochalin, V. N.; Barsoum, M. W.; Gogotsi, Y. 25th anniversary article: MXenes: a new family of two-dimensional materials. *Adv. Mater.* **2014**, *26*, 992−1005.

(10) Anasori, B.; Lukatskaya, M. R.; Gogotsi, Y. 2D metal carbides and nitrides (MXenes) for energy storage. *Nat. Rev. Mater.* **2017**, *2*, 16098.

(11) Naguib, M.; Mashtalir, O.; Lukatskaya, M. R.; Dyatkin, B.; Zhang, C.; Presser, V.; Gogotsi, Y.; Barsoum, M. W. One-step synthesis of nanocrystalline transition metal oxides on thin sheets of disordered graphitic carbon by oxidation of MXenes. *Chem. Commun.* **2014**, *50*, 7420−7423.

(12) Rakhi, R. B.; Ahmed, B.; Hedhili, M. N.; Anjum, D. H.; Alshareef, H. N. Effect of postetch annealing gas composition on the structural and electrochemical properties of Ti2CTx MXene electrodes for supercapacitor applications. *Chem. Mater.* **2015**, *27*, 5314−5323.

(13) Wang, K.; Zhou, Y.; Xu, W.; Huang, D.; Wang, Z.; Hong, M. Fabrication and thermal stability of two-dimensional carbide Ti 3 C 2 nanosheets. *Ceram. Int.* **2016**, *42*, 8419−8424.

(14) Perdew, J. P.; Burke, K.; Ernzerhof, M. Generalized gradient approximation made simple. *Phys. Rev. Lett.* **1996**, *77*, 3865−3868.

(15) Kresse, G.; Furthmüller, J. Efficient iterative schemes forab initiototal-energy calculations using a plane-wave basis set. *Phys. Rev. B: Condens. Matter Mater. Phys.* **1996**, *54*, 11169−11186.

(16) Grimme, S. Semiempirical GGA-type density functional constructed with a long-range dispersion correction. *J. Comput. Chem.* **2006**, *27*, 1787−1799.

(17) Heyd, J.; Scuseria, G. E.; Ernzerhof, M. Hybrid functionals based on a screened Coulomb potential. *J. Chem. Phys.* **2003**, *118*, 8207−8215.

(18) Wang, Y.; Lv, J.; Zhu, L.; Ma, Y. Crystal structure prediction via particle-swarm optimization. *Phys. Rev. B: Condens. Matter Mater. Phys.* **2010**, *82*, 094116.

(19) Wang, Y.; Lv, J.; Zhu, L.; Ma, Y. CALYPSO: A method for crystal structure prediction. *Comput. Phys. Commun.* **2012**, *183*, 2063−2070.

(20) Lu, S.; Wang, Y.; Liu, H.; Miao, M.-s.; Ma, Y. Self-assembled ultrathin nanotubes on diamond (100) surface. *Nat. Commun.* **2014**, *5*, 3666.

(21) Fan, D.; Lu, S.; Guo, Y.; Hu, X. Novel bonding patterns and optoelectronic properties of the two-dimensional SixCy monolayers. *J. Mater. Chem. C* **2017**, *5*, 3561−3567.

(22) Fan, D.; Lu, S.; Guo, Y.; Hu, X. Two-dimensional stoichiometric boron carbides with unexpected chemical bonding and promising electronic properties. *J. Mater. Chem. C* **2018**, *6*, 1651−1658.

(23) Togo, A.; Tanaka, I. First principles phonon calculations in materials science. *Scr. Mater.* **2015**, *108*, 1−5.

(24) Martyna, G. J.; Klein, M. L.; Tuckerman, M. Nosé-Hoover chains: The canonical ensemble via continuous dynamics. *J. Chem. Phys.* **1992**, *97*, 2635−2643.

(25) Henkelman, G.; Uberuaga, B. P.; Jónsson, H. A climbing image nudged elastic band method for finding saddle points and minimum energy paths. *J. Chem. Phys.* **2000**, *113*, 9901−9904.

(26) Zhang, Z.; Liu, X.; Yakobson, B. I.; Guo, W. Two-dimensional tetragonal TiC monolayer sheet and nanoribbons. *J. Am. Chem. Soc.* **2012**, *134*, 19326−19329.

(27) Zhao, T.; Zhang, S.; Guo, Y.; Wang, Q. TiC2: a new two-dimensional sheet beyond MXenes. *Nanoscale* **2016**, *8*, 233−242.

DOI: 10.1021/acs.jpcc.8b03425
J. Phys. Chem. C 2018, 122, 15118−15124

(28) Molina-Sánchez, A.; Wirtz, L. Phonons in single-layer and few-layer MoS2 and WS2. *Phys. Rev. B: Condens. Matter Mater. Phys.* **2011**, *84*, 155413.
(29) Cahangirov, S.; Topsakal, M.; Aktürk, E.; Şahin, H.; Ciraci, S. Two- and one-dimensional honeycomb structures of silicon and germanium. *Phys. Rev. Lett.* **2009**, *102*, 236804.
(30) Zhang, S.; Yan, Z.; Li, Y.; Chen, Z.; Zeng, H. Atomically Thin Arsenene and Antimonene: Semimetal-Semiconductor and Indirect-Direct Band-Gap Transitions. *Angew. Chem.* **2015**, *127*, 3155−3158.
(31) Wang, S.; Li, J.-X.; Du, Y.-L.; Cui, C. First-principles study on structural, electronic and elastic properties of graphene-like hexagonal Ti2C monolayer. *Comput. Mater. Sci.* **2014**, *83*, 290−293.
(32) Zhang, S.; Zhou, J.; Wang, Q.; Chen, X.; Kawazoe, Y.; Jena, P. Penta-graphene: A new carbon allotrope. *Proc. Natl. Acad. Sci. U.S.A.* **2015**, *112*, 2372−2377.
(33) Henkelman, G.; Arnaldsson, A.; Jónsson, H. A fast and robust algorithm for Bader decomposition of charge density. *Comput. Mater. Sci.* **2006**, *36*, 354−360.
(34) Grimme, S.; Antony, J.; Ehrlich, S.; Krieg, H. A consistent and accurate ab initio parametrization of density functional dispersion correction (DFT-D) for the 94 elements H-Pu. *J. Chem. Phys.* **2010**, *132*, 154104.
(35) Eames, C.; Islam, M. S. Ion intercalation into two-dimensional transition-metal carbides: global screening for new high-capacity battery materials. *J. Am. Chem. Soc.* **2014**, *136*, 16270−16276.
(36) Lindström, H.; Södergren, S.; Solbrand, A.; Rensmo, H.; Hjelm, J.; Hagfeldt, A.; Lindquist, S.-E. Li+Ion Insertion in TiO2(Anatase). 1. Chronoamperometry on CVD Films and Nanoporous Films. *J. Phys. Chem. B* **1997**, *101*, 7710−7716.
(37) Koudriachova, M. V.; Harrison, N. M.; de Leeuw, S. W. Open circuit voltage profile for Li-intercalation in rutile and anatase from first principles. *Solid State Ionics* **2002**, *152−153*, 189−194.
(38) Lunell, S.; Stashans, A.; Ojamäe, L.; Lindström, H.; Hagfeldt, A. Li and Na Diffusion in TiO2from Quantum Chemical Theory versus Electrochemical Experiment. *J. Am. Chem. Soc.* **1997**, *119*, 7374−7380.
(39) Persson, K.; Sethuraman, V. A.; Hardwick, L. J.; Hinuma, Y.; Meng, Y. S.; van der Ven, A.; Srinivasan, V.; Kostecki, R.; Ceder, G. Lithium diffusion in graphitic carbon. *J. Phys. Chem. Lett.* **2010**, *1*, 1176−1180.
(40) Çakır, D.; Sevik, C.; Gülseren, O.; Peeters, F. M. Mo2C as a high capacity anode material: A first-principles study. *J. Mater. Chem. A* **2016**, *4*, 6029−6035.
(41) Persson, K.; Hinuma, Y.; Meng, Y. S.; Van der Ven, A.; Ceder, G. Thermodynamic and kinetic properties of the Li-graphite system from first-principles calculations. *Phys. Rev. B: Condens. Matter Mater. Phys.* **2010**, *82*, 125416.
(42) Klimeš, J.; Bowler, D. R.; Michaelides, A. Chemical accuracy for the van der Waals density functional. *J. Phys.: Condens. Matter* **2009**, *22*, 022201.
(43) Klimeš, J.; Bowler, D. R.; Michaelides, A. Van der Waals density functionals applied to solids. *Phys. Rev. B: Condens. Matter Mater. Phys.* **2011**, *83*, 195131.
(44) Al Balushi, Z. Y.; Wang, K.; Ghosh, R. K.; Vilá, R. A.; Eichfeld, S. M.; Caldwell, J. D.; Qin, X.; Lin, Y.-C.; DeSario, P. A.; Stone, G.; et al. Two-dimensional gallium nitride realized via graphene encapsulation. *Nat. Mater.* **2016**, *15*, 1166.

DOI: 10.1021/acs.jpcc.8b03425
J. Phys. Chem. C 2018, 122, 15118−15124